

# Mapping and Change Assessment of Captive Limestone Mining Areas Using Landsat-5/8 Images

Venkata Sudhakar Chowdam<sup>1,2,\*</sup>, Umamaheswara Reddy Galiveeti<sup>3</sup>

<sup>1</sup>Department of Electronics and Communication Engineering, Sri Venkateswara University College of Engineering, Tirupati, India

<sup>2</sup>Department of Electronics and Communication Engineering, Sree Vidyanikethan Engineering College, Tirupati, India

<sup>3</sup>Department of Electronics and Communication Engineering, Sri Venkateswara University College of Engineering, Tirupati, India

Received 26 December 2022; received in revised form 05 April 2023; accepted 07 April 2023

DOI: <https://doi.org/10.46604/emsi.2023.11316>

## Abstract

Limestone is a non-metallic mineral extensively used in cement manufacturing and construction sector. Extensive mineral mining processes impact the environment. The study aims to map and evaluate the limestone mining area change at the Yerraguntla industrial zone in the YSR district of Andhra Pradesh, India. The normalized difference vegetation index (NDVI) and modified soil-adjusted vegetation index (MSAVI) are computed from the Landsat-5/8 images using Quantum GIS (QGIS) software. Experimental results show that the limestone mining area increases from 307 ha to 469.92 ha during 2005-2019. NDVI method is more effective than MSAVI in change assessment of limestone mining areas with overall accuracy of 87.75 % and 79.49 % and kappa coefficient of 0.89 and 0.62 respectively in 2019. The finding is compared with industry field survey reports (487.10 ha). This study contributes to the limestone mining industry management in developing a land-environmental management plan for the long-term sustainability of limestone mining.

**Keywords:** change assessment, limestone mine, remote sensing, spectral indices

## 1. Introduction

Limestone is a non-metallic mineral made up of calcium carbonate ( $\text{CaCO}_3$ ) [1]. Mineral extraction contributes nearly 2.5 % to India's gross domestic product (GDP). Limestone is an important mineral resource extensively used in the construction sector and as the primary material for cement making. In the Yerraguntla industrial zone, there is an active mining area of 487.10 ha and a reserved area of 2,226.16 ha. Both of the areas lead to a significant contribution to the socio-economic development. Limestone surface mines are developed by stripping the surface soil and vegetation to obtain minerals [1]. The removal of vegetation and the destruction of soil structure has resulted in a significant decline in biodiversity [2]. Furthermore, environmental degradation caused by mine solid waste and cement industry dust is extensive [3].

Monitoring opencast limestone mines and their solid waste is crucial to mitigate environmental impacts such as air pollution, water contamination, soil degradation, health, and the safety of surrounding communities. Moreover, monitoring is indispensable for the sustainability of limestone at the local level [4]. Conventional ground-based mine mapping methods are dependent on labor, time-consuming, and capital-intensive. Therefore, it lacks efficiency for large-scale surface mine monitoring [5].

---

\* Corresponding author. E-mail address: [sudhakar.chowdam@gmail.com](mailto:sudhakar.chowdam@gmail.com)

On the other hand, the remote sensing (RS) based mapping of limestone mines, mine transformation monitoring, and mining area environmental impact assessment is cost-effective, regular revisiting time frame, and time-saving, and it covers a broad area as well [6]. Geographical information system (GIS) is a versatile digital system for capturing, storing, visualizing, and analyzing spatial data related to geographical features [4]. The integration of RS and GIS conducts detailed mapping of limestone mining areas for decision-making, future planning, and development, which is critical for meeting the demands and wellness of the ever-growing population [7]. As a result, this study concentrates on mapping and quantitatively assessing the change in limestone mining areas by using satellite imagery and the Quantum GIS (QGIS) tool.

Previous studies [8-10] conducted research on mapping open-pit surface limestone mines using Google Earth image visual interpretation and NDVI methods. Bona et al. [11] classified limestone mining sites using multi-sensor remote sensing data and an object-based image analysis (OBIA) approach. Visual interpretation necessitates a significant amount of manual work and leads to inefficiency, especially when interpreting huge regions with numerous complex features. The algorithm based on pixel-based (PB) and object-based (OB) has revealed that classification performance is extremely subjective and dependent on training data samples [12-13]. Unlike PB and OB, an index-based classification selects satellite spectral bands for the land use/cover classification based on the land surface feature's unique spectral characteristics, making it a fast and effective mapping method. Therefore, the index-based method has better potential in mapping limestone mining areas on a large scale [4].

The purpose of the study is to map and change the assessment of the captive limestone mines at the Yerraguntla cement industrial zone in the YSR Kadapa district of Andhra Pradesh, India. Using NDVI and modified soil-adjusted vegetation index (MSAVI) spectral indices are derived from the Landsat-5/8 images for the period of 15 years (2005 to 2019), and enable to evaluate of the accuracy of the industrial field survey reports.

The article text is aligned into four sections: Section 1 describes an introduction to RS for surface mine mapping by using image classification methods and related work. While Section 2 describes the research area, and land use/cover classes in the study area, and Section 3 describes the collection of multispectral image data, pre-processing, and extraction of spectral characteristics, as well as the computation of the most widely used spectral indices such as NDVI and MSAVI. In Section 4, mining area changes are evaluated, accuracy in mapping the limestone mining area is calculated, and the limestone mining area is verified by using data from an industrial field study.

## 2. Materials

This section presents information about the study area, including geographical coordinate location, cement factories, captive limestone mineral mining region aerial and satellite images, changes in temperature, and study area distance from the district headquarters. Additionally, this section defined and described six land use and land cover classes in the study area.

### 2.1. Study area

Fig. 1 shows aerial photographs of captive limestone mines covering an area of 487.10 ha in the study region [8-10]. Mining sites were clear enough from cement industry mine field survey reports to identify and map using satellite imagery. The study area depicted in Fig. 2 is a cement industrial hotspot, with four cement industries and captive limestone mines, namely the India Cement Limited at Chilamkur and Yerraguntla, Zuari Cement Limited at Yerraguntla, Bharathi Cement Corporation Private Limited near Yerraguntla, and Kadapa Black Marble Tile Mines around Yerraguntla Mandal, YSR Kadapa district, Rayalaseema region, Andhra Pradesh, India. Yerraguntla is located 47 km west of the YSR Kadapa district headquarters.



Fig. 1 Captive limestone mines aerial photographs at the Yerraguntla zone [8]

The cement industries are located between 14.30° and 14.45° N latitude and 78.23° to 78.39° E longitude. The extreme heat of the study area reaches 48 °C in the summer (March-May), while it hovers at 14 to 27 °C in the winter (December-February) [9].

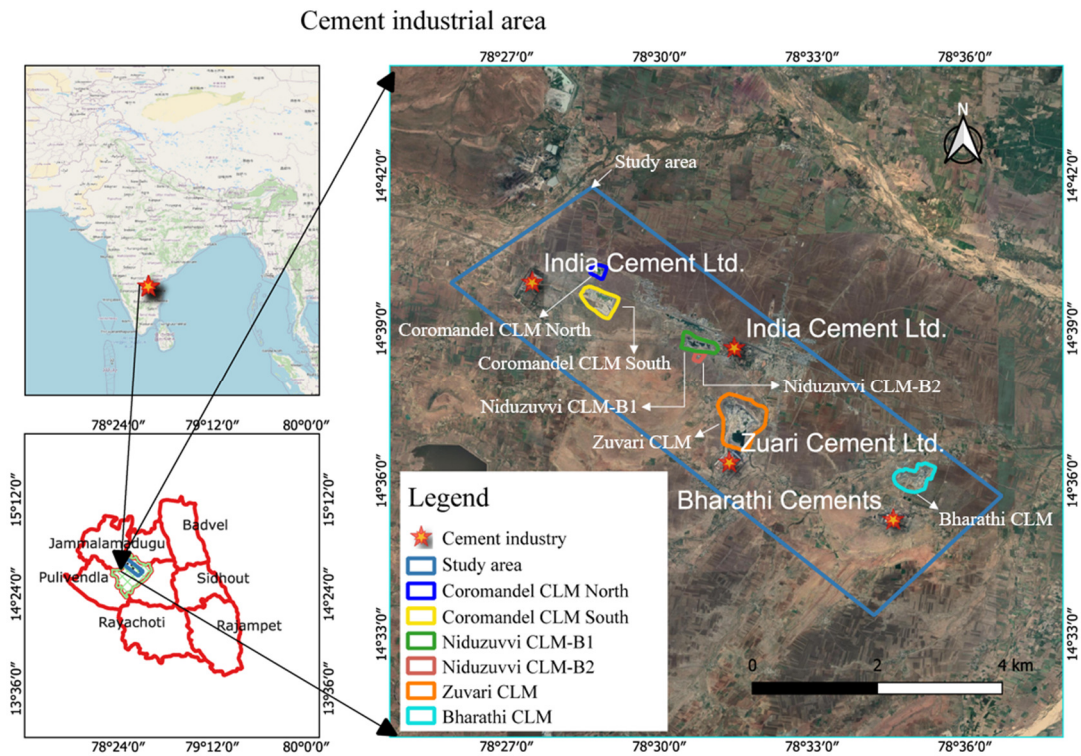


Fig. 2 Geological map of the cement industry cluster in the Yerraguntla region [8]

2.2. Land use/cover classes

Six land use/cover classes were identified from district survey reports, environmental clearance reports of limestone mines, and the cement industry’s annual reports at the Yerraguntla industrial area consisting of water bodies, limestone mines, barren lands, fallow lands, built-up, and vegetation described in Table 1 [10].

Table 1 Land surface features at the Yerraguntla industrial zone [10]

S.No.	Land class	Characterization of land features
1	Water bodies	Surface water is held in open pit mines, check dams, lakes, reservoirs, flowing streams, canals, etc.
2	Limestone mines	Surface limestone mining areas.
3	Barren lands	Land that has been dumped because of mining, erosion, or open surfaces, especially due to overgrazing and crop cultivation.
4	Fallow lands	Land that has been cleared for cultivation is allowed to remain uncultivated for one or more seasons.
5	Built-up	Buildings in both rural and urban areas, cement industry.
6	Vegetation	Natural vegetation areas that are under cultivation.

### 3. Methodology

The mapping and assessment strategy for limestone mines using geospatial indices is depicted in Fig. 3. Multispectral Landsat-5/8 image data for the years 2005 and 2019 were collected from the USGS Earth Explorer database. With the shape file, the preprocessed and layer-stacked images are clipped (subset) to the study area. Besides, to observe the spectral characteristics of land cover classes and gather ground truth data for area evaluation, a false color composite (FCC) is produced [8]. Also, the NDVI and MSAVI spectral indices were calculated by the USGS Earth Explorer database. Meanwhile, the images were reclassified using the indices' threshold values, and the mining area was evaluated and validated with industrial field survey data.

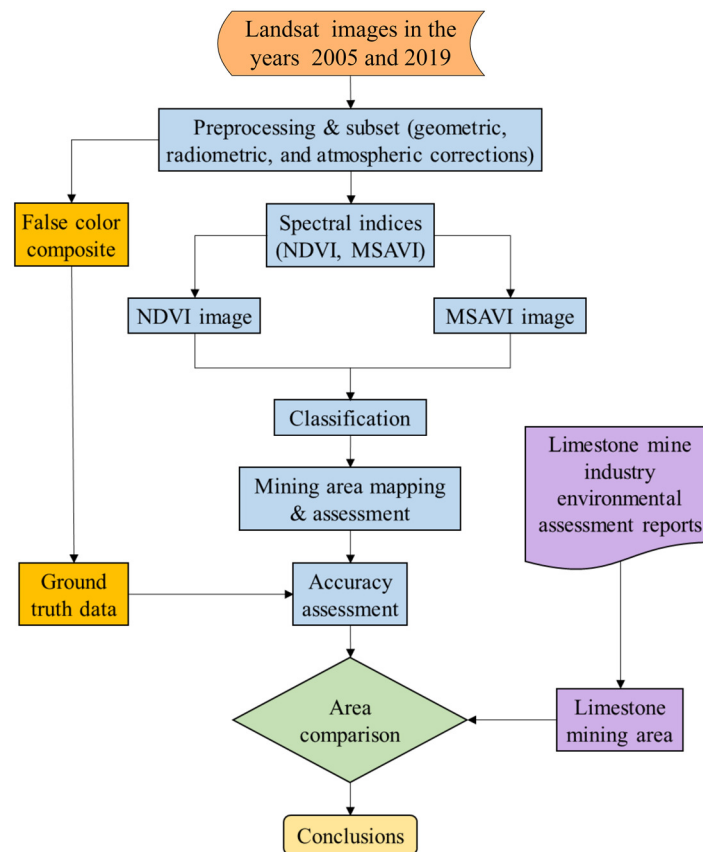


Fig. 3 Limestone mining area mapping and change assessment workflow

#### 3.1. Satellite data collection

The Earth Explorer Website of the United States Geological Survey is to accumulate multispectral satellite images for the years 2005 and 2019. Table 2 depicts the sensors used by Landsat-5/8 satellites, as well as the capture date, spatial resolution (m), earth-sun distance (AU), and sun elevation angle (Degrees). The image was chosen for its low cloud coverage (< 2 %), high quality, same season, close acquisition date, and atmospherically as well as geometrically corrected.

Table 2 Satellite imagery details are incorporated in the proposed method

Satellite	Sensor	Capture date	Spatial resolution(m)	Spectral resolution	Earth-sun distance (AU)	Sun elevation angle (Degrees)	Path/row
Landsat-8	OLI	March 6th, 2019	30	11 Bands	0.992	55.87	143/50
Landsat-5	TM	May 18th, 2005	30	8 Bands	1.012	63.64	143/50

\*Note: Operational land imager (OLI), the thematic mapper (TM)

### 3.2. Image pre-processing

With QGIS 3.18 software tool, Landsat-5 TM six spectral bands (Bands 1 to 5, and 7) with a resolution of 30 m, while Landsat-8 OLI nine spectral bands (Bands 1 to 7, and 9) with a resolution of 15 m, 30 m, and 60 m were pre-processed. All images were corrected geometrically and projected to EPSG 32644-WGS84/ UTM Zone 44N. QGIS 3.18 semi-automatic classification plug-in (SCP) was used to apply radiometric calibration and atmospheric correction to the images.

$$\rho\lambda' = M_p Q_{cal} + A_p \quad (1)$$

$$\rho_\lambda = \frac{\rho\lambda'}{\sin(\theta_{SE})} \quad (2)$$

where  $\rho\lambda'$  is the top of atmosphere (TOA) planetary reflectance, without correction for the solar angle;  $M_p$  is the band-specific rescaling factor from the metadata;  $Q_{cal}$  is the digital numbers of the band being processed;  $A_p$  is the band-specific additive rescaling factor from the metadata;  $\rho_\lambda$  is the TOA planetary reflectance, with correction for the solar angle;  $\theta_{SE}$  is the sun elevation angle (in degrees) from metadata.

During the radiometric calibration, raw digital data (digital numbers) values of the satellite bands were converted into TOA transmittance using Eqs. (1)-(2) [8-10]. An image-based atmospheric correction using the dark-object subtraction 1 (DOS1) method was implemented in SCP. A true-color composite image of the study area obtained by the Landsat satellite is shown in Fig. 4. The image shows the limestone mines in white, barren lands in blue, fallow lands in dark brown, mine solid waste in light grey, and vegetation in green. In true color composite (TCC) images, land, and water are not much clearer, and vegetation does not reflect strongly. However, these are strong in the infrared (IR) than in the visible. Thus, FCC is better for visual interpretation of land surface features.

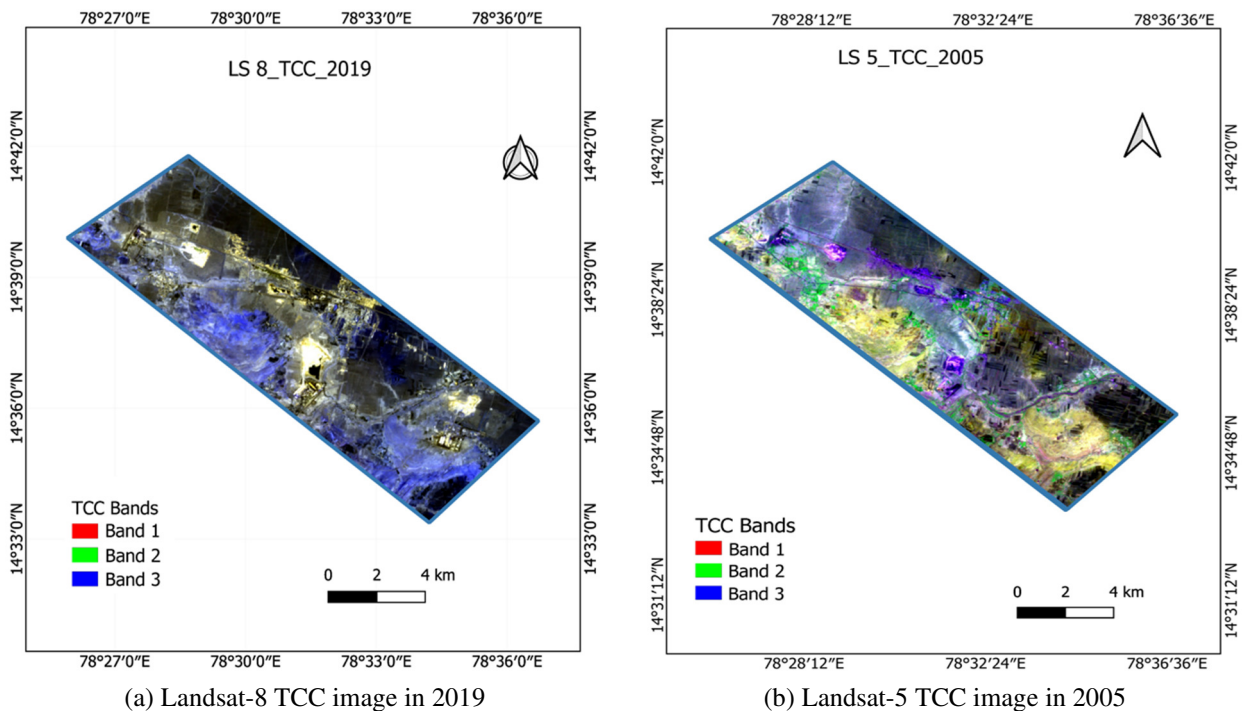


Fig. 4 Landsat satellite true color composite image of the study area

### 3.3. Spectral characteristics of land cover features

The spectral signature properties of land use/cover classes are obtained using SCP in the QGIS tool [14]. The spectral signatures of limestone and other land use/cover classes are depicted in Fig. 5 in the visible (0.4 to 0.7  $\mu\text{m}$ ), near-infrared (NIR) (0.78 to 1.4  $\mu\text{m}$ ), and short-wave infrared (SWIR) (1.4 to 3.0  $\mu\text{m}$ ) portions of the electromagnetic (EM) spectrum. The spectral signature values of all land use/cover classes are unique to the substance and environment in which they are assessed. Limestone reflected visible and near-infrared (VNIR) light while absorbing SWIR radiation at the 1.4  $\mu\text{m}$  wavelengths in the study area.

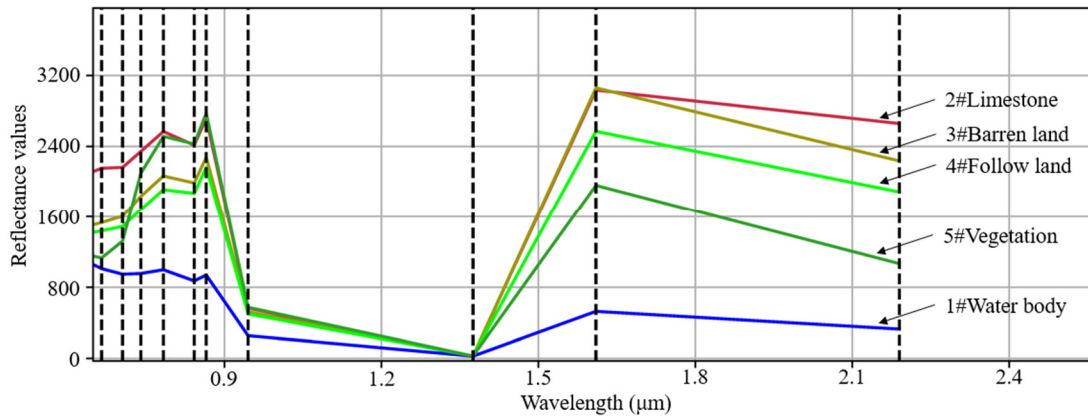


Fig. 5 Spectral characteristics of land use/cover classes in the study area [6]

### 3.4. False color composite images for ground truth data

Satellite multispectral bands converted to reflectance were clipped to the region of interest (ROI) using the study area shape file. From the clip of layers, a layer stack image was generated using the nearest neighbor resampling algorithm for the creation of color composites. Fig. 6 depicts the result of the color composite. The band composite 7-6-2 for Landsat-8 and the band composite 7-5-1 for Landsat-5 are useful for the interpretation of the geological formations and lithology features. Ground truth data of six land use/cover categories were collected using Landsat-8 image FCC by the on-screen digitization and visual image interpretation techniques in the QGIS tool.

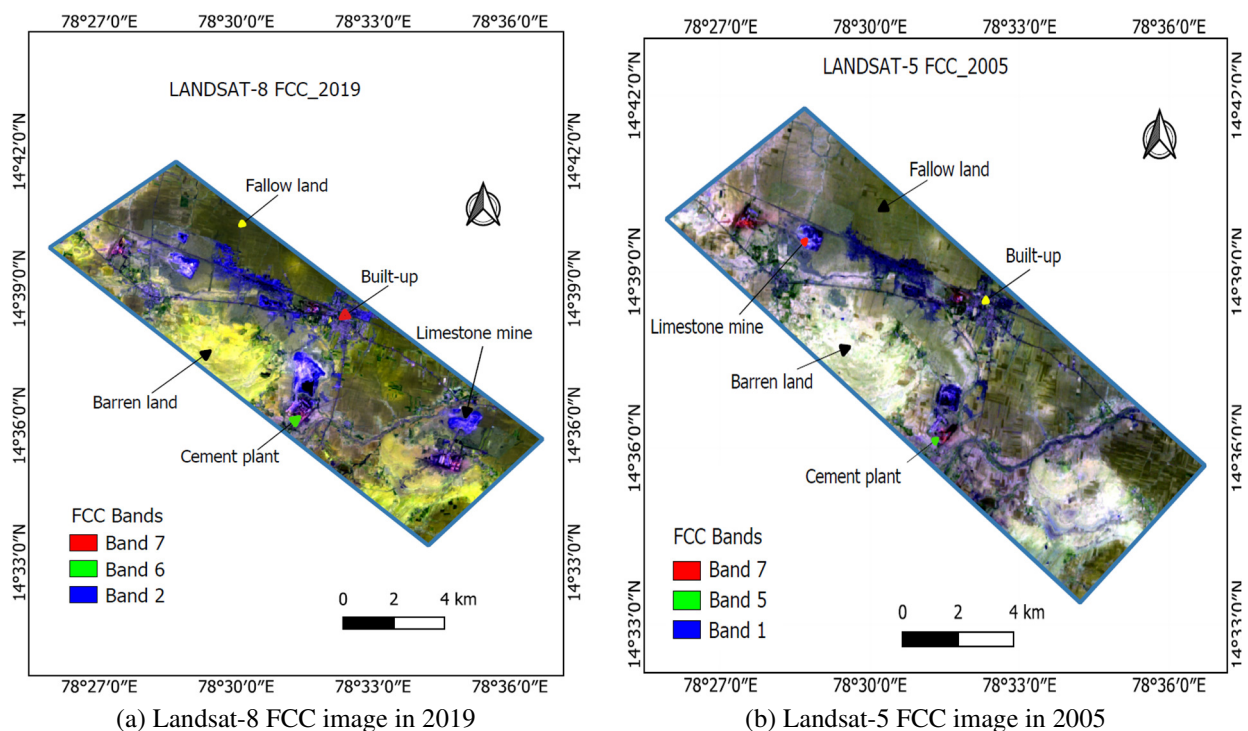


Fig. 6 Major land cover classes interpretation in the FCC

### 3.5. Spectral indices

Spectral indices are the radiometric dimensionless quantity computed from two or more spectral bands in a satellite image. Spectral indices are used to highlight pixels that show the relative plenty or lack of a land-use/cover type of interest in an image that cannot be observed in the display of the original color bands [15]. Vegetation indices such as NDVI and MSAVI are the most popular type used for mapping major geological land surface features. Other indices such as bare soil index (BSI), normalized difference built-up index (NDBI), and weighted normalized difference water index (WNDWI) are used for bare soil, man-made (built-up) features, and water bodies mapping on the land surface respectively. In this study, NDVI and MSAVI were computed for mapping and the change assessment of the limestone mining area, as well as mapping of water bodies, barren lands, fallow lands, built-up, and vegetation in the study area using their spectral characteristics (Fig. 5 and bands listed in Table 3).

Table 3 Landsat satellite band designation and their usage in land feature identification

Band	LS-5TM ( $\mu\text{m}$ )	LS-8 OLI ( $\mu\text{m}$ )	Band usages
Blue	B1 (0.45-0.52)	B2 (0.45-0.51)	Identification of man-made characteristics, differentiation of vegetation kinds, and mapping of different forest types.
Green	B2 (0.52-0.60)	B3 (0.53-0.59)	It highlights peak vegetation and provides a great contrast between pure and turbid (muddy) water.
Red	B3 (0.63-0.69)	B4 (0.64-0.67)	Recognizing different soil types, urban features, and vegetation types.
NIR	B4 (0.77-0.90)	B5 (0.85-0.88)	Plant health is assessed with a focus on shorelines and biomass content.
SWIR1	B5 (1.55-1.75)	B6 (1.57-1.65)	Distinguishing between the soil's and the vegetation's relative levels of moisture, and differentiation between rocks and soils.
SWIR2	B7 (2.09-2.35)	B7 (2.11-2.29)	Moisture levels in plants, soil, and hydrothermally changed rocks around mineral deposits.

#### 3.5.1. Normalized difference vegetation index

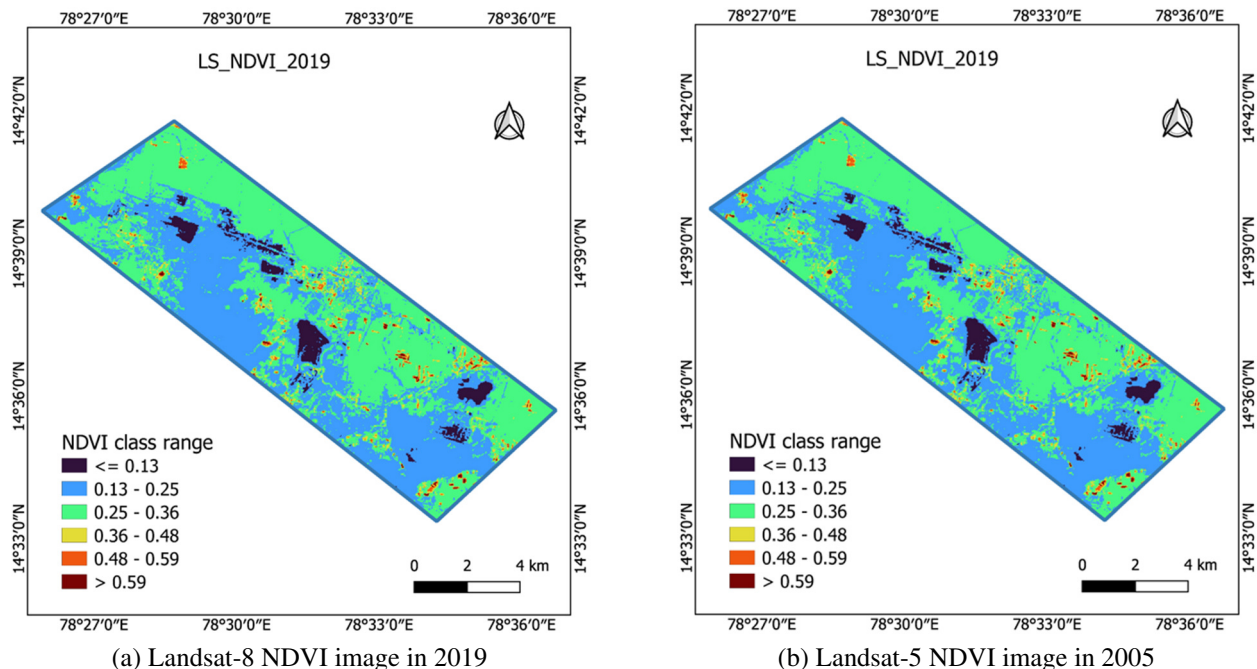


Fig. 7 NDVI-discrete interpolation outcome in 2005 and 2019

The normalized difference vegetation index (NDVI) with multi-spectral RS data was used to identify land use/cover classes [9, 16].

$$\text{NDVI} = \frac{\text{NIR} - \text{Red}}{\text{NIR} + \text{Red}} \quad (3)$$

The NDVI computed from the NIR and red bands (Eq. 3) of Landsat-5 ( $0.07 \leq \text{NDVI} < 0.29$ ) in 2005, while the NDVI range ( $0.13 \leq \text{NDVI} < 0.59$ ) obtained in 2019 with Landsat-8. The NDVI positive values ( $\leq 0.13$ ) indicate limestone mining areas, 0.13 to 0.25 represents barren lands, 0.25 to 0.36 stands for fallow lands, and 0.36 to 0.59 is for built-up and vegetated areas. Finally,  $\text{NDVI} > 0.59$  indicates dense vegetation features [17] in 2019 as shown in Fig. 7. The images were taken during the summer for mapping the limestone mining area. Hence most of the agricultural fields around the mining regions were marked as bare soil (fallow lands) and had little vegetation. Since the NDVI is sensitive to soil backdrops and only detects healthy vegetation, it will not accurately display areas with scant vegetation or bare soil.

### 3.5.2. Soil-adjusted vegetation index

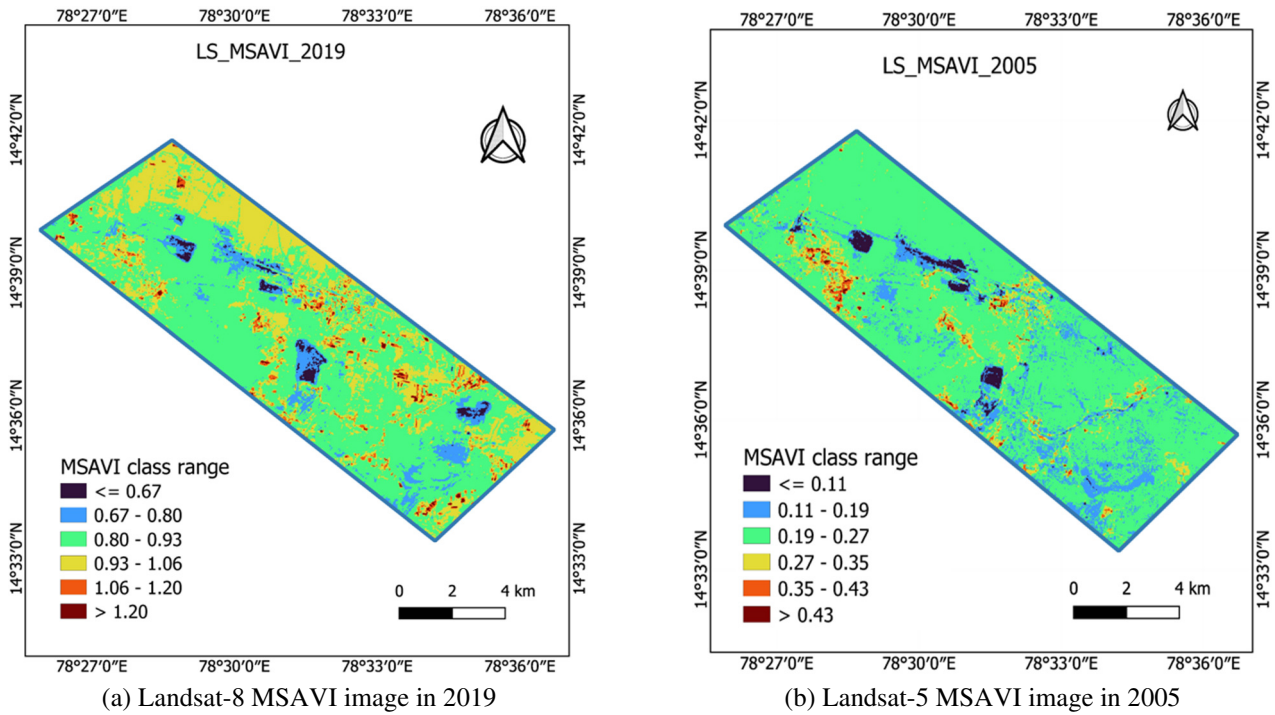


Fig. 8 MSAVI-discrete interpolation outcome for the years 2005 and 2019

In arid areas with limited vegetation cover, the soil-adjusted vegetation index (SAVI) is used to adjust NDVI to minimize the effects of soil brightness using a soil-brightness coefficient ( $L$ ). The outputs of the index range from -1.0 to 1.0.

$$\text{SAVI} = \frac{(1+L)(\text{NIR} - \text{Red})}{(\text{NIR} + \text{Red}) + L} \quad (4)$$

The  $L$  factor ranges from 0 to 1 and varies inversely with the quantity of vegetation present.  $L = 1$  in the absence of any green vegetation,  $L = 0.5$  in the presence of some green vegetation but not much, and  $L = 0$  in the presence of a lot of green vegetation, which is comparable to the NDVI method [18].

$$\text{WDVI} = \text{NIR} - (a \times \text{Red}) \quad (5)$$

where  $a = \text{NIR}_{\text{soil}} / \text{Red}_{\text{soil}}$ .

An MSAVI transforms the coefficient  $L$  in the SAVI (Eq. 4) with a variable  $L$  function [19]. The  $L$  function is derived from induction or by combining the NDVI, and the weighted difference vegetation index (WDVI), which can be shown in Eq. 5.

$$\text{MSAVI} = \frac{(2 \times \text{NIR} + 1) - \sqrt{(2 \times \text{NIR} + 1)^2 - 8 \times (\text{NIR} - \text{Red})}}{2} \quad (6)$$



The MSAVI was computed as the ratio of NIR and Red band values, with an inductive L factor used to minimize soil implications on the vegetation. The MSAVI as shown in Eq. 6, increases the vegetation index dynamic range, while decreasing soil background influences, resulting in increased vegetation sensitivity [18]. Fig. 8 shows the MSAVI computed in 2005 and 2019. The index figures are unable to discriminate between built-up and barren lands. In 2019, the limestone mine index range was from 0.67 to 0.8, barren lands range was from 0.8 to 0.93, and fallow lands range was from 0.93 to 1.06.

### 4. Results and Discussion

The NDVI has been widely used to analyze changes in vegetation growth rate. NDVI and MSAVI are also effective for mapping and determining the area change of limestone mines using spectral index threshold values. Table 4 depicts the captive limestone mining areas between 2005 and 2019. Fig. 9 and Fig. 10 depict the LULC classes using NDVI and MSAVI, respectively, followed by an accuracy assessment in Table 5 and a comparison of limestone mining area land use change in Fig. 11.

#### 4.1. Limestone mining area assessment

The study evaluates the active limestone mining area spatiotemporal change at the Yerraguntla industrial zone. The land use/cover classes were determined by the classification of NDVI images using the “reclassify by table” tool in the system for automated geoscientific analyses (SAGA) GIS software. The assessed limestone mining area quantitative values are outlined in Table 4. The classified images are depicted in Fig. 9 and Fig. 10. The findings from the NDVI method denote that the limestone mining area increased from 307 ha in 2005 to 469.92 ha in 2019. By using the MSAVI technique, the mining area of limestone grew from 221 ha in 2005 to 301 ha in 2019. The results of the analysis show that there was a change in some ground classes such as the increase in barren lands (from 1061 to 4874 ha) and the drop in fallow lands (from 9424 to 5392 ha) from 2005 to 2019.

Table 4 Limestone mining area change from the year 2005 to 2019

S.No.	Classification method	Limestone mine area (ha)	
		2005 (yr)	2019 (yr)
1	NDVI	307	469.92
2	MSAVI	221	568.62

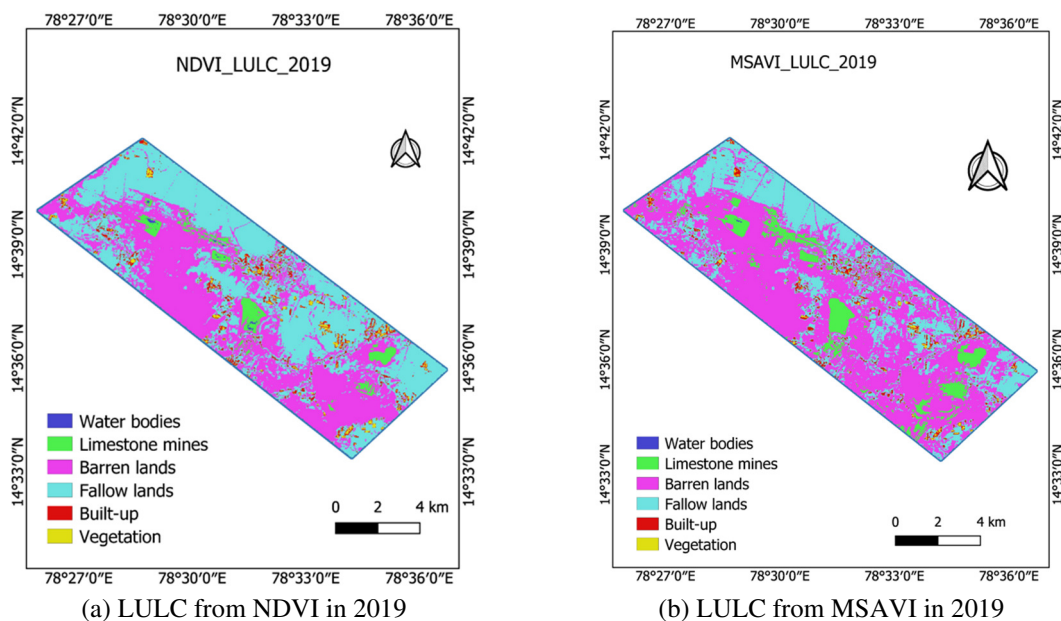


Fig. 9 Land use land cover (LULC) maps at the limestone mining area in 2019

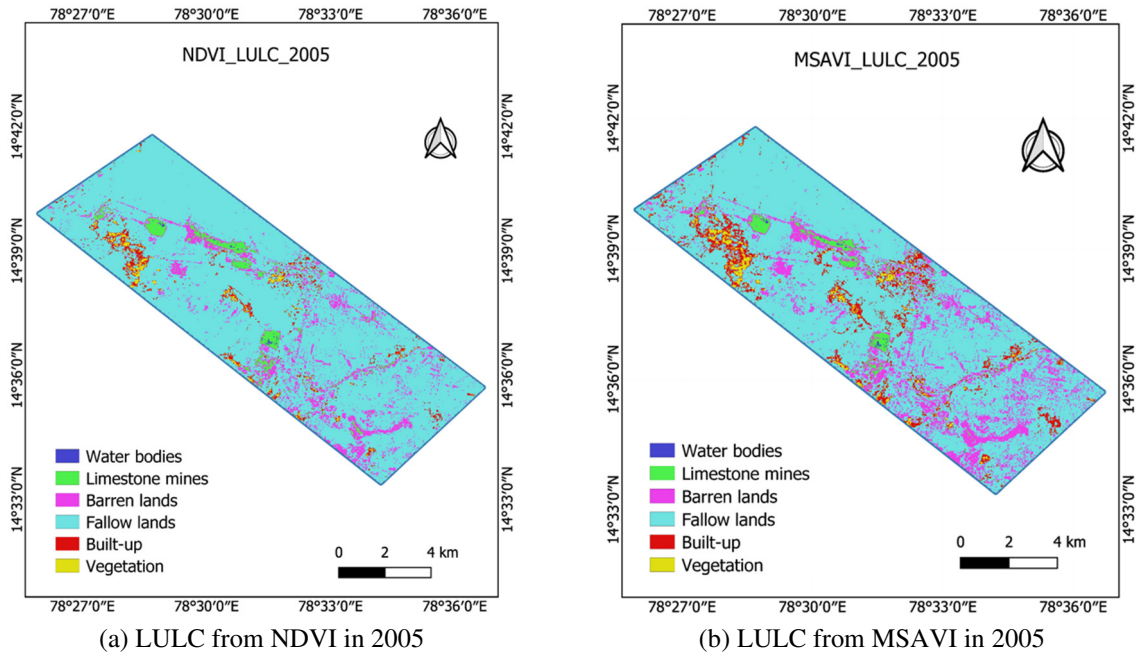


Fig. 10 Land uses land cover (LULC) maps at the limestone mining area in 2005

#### 4.2. Accuracy assessment

Estimating the accuracy of LULC classifications is vital for evaluating the quality of findings. The accuracy assessment was conducted by the construction of an error matrix using the QGIS semi-automatic classification plugin (SCP) accuracy assessment tool.

$$PA = \frac{\text{Number of correctly classified pixels of a class}}{\text{sum producer in a column}} \quad (7)$$

$$UA = \frac{\text{Number of correctly classified pixels of a class}}{\text{sum user in a row}} \quad (8)$$

$$OA = \frac{\text{sum of correctly classified pixels}}{\text{sum of pixels used for accuracy assessment}} \quad (9)$$

$$\text{Kappa hat} = \frac{(N \times A) - B}{N^2 - B} \quad (10)$$

where  $N$  is the total number of pixels used for accuracy evaluation,  $A$  is the total number of correctly classified pixels, and  $B$  is the product of the total ground truth data for a class.

The statistical metrics such as user's accuracy (UA), producer's accuracy (PA), overall accuracy (OA), and Kappa hat [12] were computed using the Eqs. (7)-(10). The result of accuracies is summarized in Table 5. The NDVI reclassification results show a considerable OA of 87.75 % and a Cohen's kappa hat of 0.89 in 2019. In 2005, the limestone mine land use class had the lowest PA of 24.17 % and UA of 50.97 %. The MSAVI reclassification results show a considerable OA of 79.49 % and a Cohen's kappa hat of 0.62 in 2019. In 2005, the limestone class had the lowest PA of 19.53 % and UA of 56.64 %.

Table 5 Limestone mines mapping accuracy and area in the years 2005 and 2019

Spectral index	2019					2005				
	PA (%)	UA (%)	OA (%)	Kappa hat	Area (ha)	PA (%)	UA (%)	OA (%)	Kappa hat	Area (ha)
NDVI	94.54	89.96	87.75	0.89	469.92	24.17	50.97	46.35	0.16	307
MSAVI	100	64.13	79.49	0.62	568.62	19.53	56.64	49.33	0.54	221

### 4.3. Comparison of mining area change

The classification results were compared with delineated high-resolution (1m/pixels) Google Earth image (486.47 ha) and industry field survey reports (487.10 ha) in 2019 [8-10]. As shown in Fig. 11. The comparison results revealed that the mining area computed by using the NDVI method is highly precise to industrial field survey data. The limestone mining area increased from 307 ha in 2005 to 469.92 ha in 2019. Due to the increased limestone production [19-21], the growth in the mining area meets the raw material requirements of India Cement Limited at Chilamkur and Yerraguntla, ZuariCement Limited at Yerraguntla, and Bharathi Cement Corporation Private Limited at Yerraguntla industrial area.

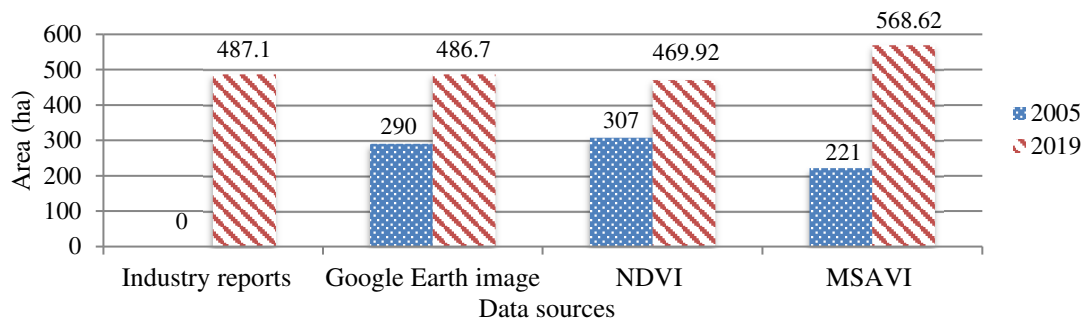


Fig. 11 Limestone mining area Land use change comparison

## 5. Conclusion

This research demonstrates the application of NDVI and MSAVI indices in mapping the limestone mining area and the change assessment from 2005 to 2019. The study found the limestone mining area increased from 307 ha to 469.92 ha. While barren lands increased (from 1,061 ha to 4,874 ha), and fallow lands decrease (from 9,424 ha to 5,392 ha) from 2005 to 2019 respectively. The results indicate the NDVI method is more reliable for monitoring and the change assessment of the limestone mining area than the MSAVI method. The change assessment by using RS methods is beneficial to policymakers in understanding and decision-making on the mining-induced LULC change and the environmental impacts. The spectral characteristics of limestone solid waste, building material, and barren rocks are too similar to separate them adequately by using spectral index-based techniques. For future work, hyperspectral image classification utilizing machine learning techniques is concerned with LULC classification in the research region.

## Acknowledgments

The authors are grateful to the limestone mine and cement industry management for allowing the researchers to conduct fieldwork in the study area.

## Conflicts of Interest

The authors declare no conflict of interest.

## References

- [1] A. T. Lima, K. Mitchell, D. W. O'Connell, J. Verhoeven, and P. V. Cappellen, "The Legacy of Surface Mining: Remediation, Restoration, Reclamation and Rehabilitation," *Environmental Science & Policy*, vol. 66, pp. 227-233, December 2016.
- [2] R. C. Rooney, S. E. Bayley, and D. W. Schindler, "Oil Sands Mining and Reclamation Cause Massive Loss of Peatland and Stored Carbon," *Proceedings of the National Academy of Sciences*, vol. 109, no. 13, pp. 4933-4937, March 2012.
- [3] S. Li, J. Wu, Y. Huo, X. Zhao, and L. Xue, "Profiling Multiple Heavy Metal Contamination and Bacterial Communities Surrounding an Iron Tailing Pond in Northwest China," *Science of the Total Environment*, vol. 752, article no. 141827, January 2021.

- [4] S. Gao, Y. Chen, K. Li, Y. Li, J. Yu, and R. Rao, "Mapping Opencast Iron Mine and Mine Solid Waste Based on a New Spectral Index from Medium Spatial Resolution Satellite Data," *IEEE Journal of Selected Topics in Applied Earth Observations and Remote Sensing*, vol. 14, pp. 7788-7798, 2021.
- [5] J. Li, Y. Pei, S. Zhao, R. Xiao, X. Sang, and C. Zhang. "A Review of Remote Sensing for Environmental Monitoring in China," *Remote Sensing*, vol. 12, no. 7, article no. 1130, April 2020.
- [6] A. A. Pericak, C. J. Thomas, D. A. Kroodsma, M. F. Wasson, M. R. V. Ross, N. E. Clinton, et al., "Mapping the Yearly Extent of Surface Coal Mining in Central Appalachia Using Landsat and Google Earth Engine," *Plos One*, vol. 13, no. 7, article no. e0197758, 2018.
- [7] Andhra Pradesh Space Applications Centre, "District Survey Report—Ysr Kadapa District," Department of Mines and Geology Government of Andhra Pradesh, District Survey Report, July 2021.
- [8] C. V. Sudhakar, G. U. Reddy, and N. U. Rani, "Delineation and Evaluation of the Captive Limestone Mining Area Change and Its Influence on the Environment Using Multispectral Satellite Images for Industrial Long-Term Sustainability," *Cleaner Engineering and Technology*, vol. 10, article no. 100551, October 2022.
- [9] C. V. Sudhakar and G. U. Reddy, "Satellite Image Based Spatio-Temporal Variation Assessment in Captive Limestone Mines for Long-Term Viability," *Journal of Mobile Multimedia*, vol. 18, no. 3, pp. 635-660, January 2022.
- [10] C. V. Sudhakar and G. U. Reddy, "Land Use Land Cover Change Assessment at Cement Industrial Area Using Landsat Data-Hybrid Classification in Part of YSR Kadapa District, Andhra Pradesh, India," *International Journal of Intelligent Systems and Applications in Engineering*, vol. 10, no. 1, pp. 75-86, March 2022.
- [11] D. S. Bona, A. M. Arymurthy, and P. Mursanto, "Classification of Limestone Mining Site Using Multi-Sensor Remote Sensing Data and OBIA Approach a Case Study: Biak Island, Papua," *International Conference on Advanced Computer Science and Information Systems*, pp. 417-422, October 2018.
- [12] D. Paull, G. Banks, C. Ballard, and D. Gillieson, "Monitoring the Environmental Impact of Mining in Remote Locations through Remotely Sensed Data," *Geocarto International*, vol. 21, no. 1, pp. 33-42, 2006.
- [13] S. Bürck, "Remote Sensing Analyses for Open Pit Mine Area Computation. A Comparative Study on the Implementation of Multi-Spectral Classifications and Crowdsourcing to Compute the Spatial Extent of Four Open-Pit Mines in Indonesia, Australia, Canada and Brazil," Ph.D. dissertation, Faculty of Chemistry and Earth Sciences, Institute of Geography, Heidelberg University, Heidelberg, 2020.
- [14] S. Rajendran, S. Nasir, M. A. El-Ghali, K. Alzebdah, A. S. Al-Rajhi, and M. Al-Battashi, "Spectral Signature Characterization and Remote Mapping of Oman Exotic Limestones for Industrial Rock Resource Assessment," *Geosciences*, vol. 8, no. 4, article no. 145, April 2018.
- [15] V. S. D. Silva, G. Salami, M. I. O. D. Silva, E. A. Silva, J. J. M. Junior, and E. Alba, "Methodological Evaluation of Vegetation Indexes in Land Use and Land Cover (LULC) Classification," *Geology, Ecology, and Landscapes*, vol. 4, no. 2, pp. 159-169, 2020.
- [16] G. M. Gandhi, S. Parthiban, N. Thummalu, and A. Christy, "NDVI: Vegetation Change Detection Using Remote Sensing and GIS – A Case Study of Vellore District," *Procedia Computer Science*, vol. 57, pp. 1199-1210, 2015.
- [17] A. Madasa, I. R. Orimoloye, and O. O. Ololade, "Application of Geospatial Indices for Mapping Land Cover/Use Change Detection in a Mining Area," *Journal of African Earth Sciences*, vol. 175, article no. 104108, March 2021.
- [18] J. Qi, A. Chehbouni, A. R. Huete, Y. H. Kerr, and S. Sorooshian, "A Modified Soil Adjusted Vegetation Index," *Remote Sensing of Environment*, vol. 48, no. 2, pp. 119-126, May 1994.
- [19] C. Fan, B. He, P. Kong, H. Xu, Q. Zhang, and X. Quan, "Predicting 1-H Dead Fuel Moisture Content at Regional Scales Using Machine Learning from Himawari-8 Data," *IEEE International Geoscience and Remote Sensing Symposium IGARSS*, pp. 1222-1225, July 2021.
- [20] D. Poursanidis, N. Chrysoulakis, and Z. Mitraka, "Landsat 8 vs. Landsat 5: A Comparison Based on Urban and Peri-Urban Land Cover Mapping," *International Journal of Applied Earth Observation and Geoinformation*, vol. 35, no. part B, pp. 259-269, March 2015.
- [21] C. V. Sudhakar, G. U. Reddy, and N. U. Rani, "In Situ Measurement and Management of Soil, Air, Noise and Water Pollution in and Around the Limestone Mining Area of Yerraguntla, YSR Kadapa, Andhra Pradesh, India for the Sustainable Development," *Journal of Applied and Natural Science*, vol. 14, no. 3, pp. 746-761, 2022.

